DMD Fast Forward. Published on May 6, 2009 as doi:10.1124/dmd.109.026658

SEMI-PHYSIOLOGICALLY-BASED PHARMACOKINETIC MODELS FOR THE INHIBITION OF MIDAZOLAM CLEARANCE BY DILTIAZEM AND ITS MAJOR METABOLITE

Xin Zhang[1], Sara K. Quinney[2], J Christopher Gorski[3], David R. Jones, and Stephen D. Hall[1]

Division of Clinical Pharmacology, Department of Medicine, Indiana University School of Medicine, Indianapolis, IN (S.K.Q., J.C.G., D.R.J., and S.D.H.)

Department of Pharmacy Practice, School of Pharmacy and Pharmaceutical Sciences, Purdue University, Indianapolis, IN (X.Z.)

Running Title: Prediction of CYP3A4 inhibition by diltiazem and its major metabolite

Address Correspondence to: Stephen D. Hall, Ph.D

Eli lilly and Company

Lilly Corporate Center

Drop Code 0720

Indianapolis, IN 46285

Phone: 317-277-0338

Fax: 317-433-9287

E-mail: hallst@lilly.com

Text page: 34

Tables: 4

Figures: 7

References: 46

Abstract: 257 words

Introduction: 765 words

Discussion: 1447 words

Abbreviations used are: DTZ: diltiazem; nd-DTZ: N-desmethyldiltiazem; CYP3A4: cytochrome P450 3A4; $AUC_{0-\infty}$: area under the plasma concentration-time curve from zero to infinity; MDZ: midazolam; PK: pharmacokinetic; PBPK: physiologically-based pharmacokinetic; IR: immediate-release; SR: slow-release; DDIs: drug-drug interactions; HLM: human liver microsome.

DMD Fast Forward. Published on May 6, 2009 as DOI: 10.1124/dmd.109.026658
This article has not been copyedited and formatted. The final version may differ from this version.

Abstract

Prediction of the extent and time course of drug-drug interactions (DDIs) between the mechanism-based inhibitor diltiazem (DTZ), and the CYP3A4 substrate midazolam (MDZ) is confounded by time- and concentration-dependant clearance of the inhibitor. Semi-physiologically-based pharmacokinetic (PBPK) models were developed for DTZ and MDZ with the major metabolite of DTZ, N-desmethyldiltiazem (nd-DTZ), incorporated in the DTZ model. Enzyme kinetic parameters (k_{inact} and K_I) for DTZ and nd-DTZ were estimated *in vitro* and used to model the time course of changes in the amount of CYP3A4 in the liver and gut wall, which in turn, determined the nonlinear elimination of MDZ and DTZ, and the corresponding DDI. The robustness of the model prediction was assessed by comparing the results of the prediction to published DTZ pharmacokinetic and DTZ/MDZ interaction data. A clinical study was conducted to further validate the predicted increase of MDZ exposure following DTZ treatment. The model predicted the nonlinear disposition of DTZ following single and multiple oral doses. The clinical study showed that DTZ treatment resulted in 4.1-fold and 1.6-fold increases in MDZ exposure following oral and intravenous MDZ administration, respectively, suggesting that the DDI in the gut wall plays an important role in the DTZ/MDZ interaction. The semi-PBPK model incorporating DDI at the gut wall and the effect of nd-DTZ successfully predicted the nonlinear disposition of DTZ and its interaction with MDZ. Moreover, model simulation suggested both DTZ and nd-DTZ contributed to the overall inhibitory effect following DTZ administration, and the values of the *in vitro* estimated inhibition parameters and CYP3A4 turnover rate are critical for the prediction.

DMD Fast Forward. Published on May 6, 2009 as DOI: 10.1124/dmd.109.026658
This article has not been copyedited and formatted. The final version may differ from this version.

Introduction

Diltiazem (DTZ), a benzothiazepine derivative, is a widely used calcium channel blocker in the therapy of angina pectoris and hypertension (Chaffman and Brogden, 1985; Buckley et al., 1990). In humans, the pharmacokinetic properties of DTZ are characterized by intermediate bioavailability with large variation (25-73%), intermediate-high clearance (11.5-21.3 ml/min/kg), extensive plasma protein binding (77-86%), and a large volume of distribution (3-8 L/kg) (Piepho et al., 1982; Hermann et al.,, 1983; Bianchetti et al., 1991). DTZ undergoes extensive metabolism, with only 0.1-4% of the dose excreted unchanged in the urine (Rovei et al., 1980). The major metabolites in human include N-desmethyldiltiazem (nd-DTZ), deacetyldiltiazem, and N-desmethyl,deacetyldiltiazem (Rovei et al., 1980). The N-desmethyl and deacetylated metabolites are present in concentrations of 30 and 10% of parent, respectively (Rovei et al., 1980).

DTZ displays nonlinear disposition in humans, and metabolism of DTZ has been suggested to be saturable at clinically relevant concentrations despite the fact that saturation is not expected based on the *in vitro* Km value of DTZ (~ 3uM) (Zelis and Kinney, 1982; Smith et al., 1983; Jones et al.,1999). The area under the plasma concentration time curve from zero to infinity ($AUC_{0-\infty}$) increases disproportionally after increased single oral doses of DTZ. Moreover, the steady-state plasma concentration is not predictable from that after single dose using dose independent models of disposition (Buckley et al., 1990). Multiple-dose administration results in a 60% reduction in oral clearance of DTZ, however, with no significant change in the terminal half life (Lefebvre et al., 1994).

DTZ is a clinically significant inhibitor of cytochrome P450 3A4 (CYP3A4). Therapeutically important interactions between oral diltiazem and midazolam (MDZ) (Backman et al., 1994), triazolam (Varhe et al., 1996), cyclosporine (Wagner et al.,

1988), lovastatin (Azie et al., 1998; Masica et al., 2000), and carbamazepine (Brodie and MacPhee, 1986; Eimer and Carter, 1987) have been documented. A previous study by our group also demonstrated that DTZ (120 mg twice daily for seven days) caused a 62% decrease in small bowel CYP3A4 activity (Pinto et al., 2005). Thus irreversible inhibition of CYP3A by DTZ is the most likely explanation for the nonlinear pharmacokinetics of DTZ.

DTZ inhibits CYP3A4 mainly as a mechanism-based inhibitor through metabolic intermediate complex formation as demonstrated by *in vitro* studies (Jones et al., 1999). Various approaches have been applied for the prediction of *in vivo* DDIs involving mechanism-based inhibitors (Kanamitsu et al., 2000; Mayhew et al., 2000; Takanaga et al., 2000; Ito et al., 2003; Wang et al., 2004; Venkatakrishnan and Obach, 2005). However, despite several successful predictions, these approaches either do not address the change in inhibitor concentration with time, or do not consider the interaction at the site of gut wall. Furthermore, no effect of active metabolites has ever been incorporated in the model development, largely due to lack of information on metabolite disposition in the literature.

A recent *in vitro* study suggested nd-DTZ may play an important role in the interactions between DTZ and other CYP3A4 substrates at a pharmacokinetic level. It has been shown that nd-DTZ is a more potent inhibitor of CYP3A4 than the parent drug *in vitro*, as both reversible and irreversible inhibitor (Sutton et al., 1997; Mayhew et al., 2000). However, the steady-state plasma concentration of nd-DTZ is about one third of that of DTZ and its pharmacological effect as a coronary vasodilator is about one fifth of that of DTZ (Hermann and Morselli, 1985). Therefore, given the higher inhibition potency but lower exposure of nd-DTZ compared to DTZ, it is not clear whether nd-DTZ contributes to the overall inhibitory effect observed *in vivo* after DTZ administration.

Here we present the development and validation of a semi-physiologically-based pharmacokinetic (PBPK) model for the prediction of the nonlinear disposition of DTZ and its interaction with MDZ. DDI in the gut wall and liver, plasma concentration–time profile of the metabolite, nd-DTZ, and CYP3A4 enzyme pools were incorporated in the model. Furthermore, the only DTZ/MDZ interaction data available in literature is for the immediate-release (IR) preparation of DTZ, where only changes in the AUC after oral MDZ administration was investigated (Backman et al., 1994). A clinical study was conducted to quantify the extent of the interaction between MDZ and the most commonly used slow release (SR) preparation of DTZ (Cardizem SR™, Biovail Pharmaceuticals, Ontario, Canada). The robustness of the model prediction was assessed by comparing the results of the prediction to published DTZ PK and DTZ/MDZ data, and was further validated with the results of our prospective clinical study of DTZ/MDZ interaction. Simulation was conducted to evaluate the relative contribution of DTZ and nd-DTZ to the overall inhibition of CYP3A4 as probed by MDZ AUC fold increases. The sensitivity of the model prediction to several key parameters was also evaluated.

DMD Fast Forward. Published on May 6, 2009 as DOI: 10.1124/dmd.109.026658
This article has not been copyedited and formatted. The final version may differ from this version.

Materials and Methods

PBPK models were developed for DTZ and MDZ, separately, based on the reported PK and physiological parameters (Table 1 and 2). CYP3A4 enzyme pools in liver and gut wall, the sites for the interaction between DTZ and MDZ, were modeled as separate compartments (Figure 1). The gut and hepatic availability and systemic clearance of each drug were expressed as functions of intrinsic clearance, which was related to the amount of active CYP3A4 in gut wall and liver. Therefore, the time-dependant change in the amount of active CYP3A4 determined the nonlinear disposition of DTZ and DTZ/MDZ interaction.

PBPK model development

The PBPK models for DTZ and MDZ (Figure 1) were identical except that the DTZ model recognized the generation of an inhibitory metabolite, nd-DTZ. For MDZ, a conventional two-compartment PK model with additional compartments for gut lumen, gut wall, portal vein, and liver were developed. Based on the model, the mass balance equations for drugs transferring between compartments are expressed as following:

$$dA_{CENT}/dt = -(C_{CENT}\times V_{CENT}\times k_{12})+C_{PER}\times V_{PER}\times k_{21}+Q_H\times C_{LIV}-Q_{PV}\times C_{CENT}-Q_{HA}\times C_{CENT}-C_{CENT}\times CL_{REN} \quad (1)$$

$$dA_{PER}/dt = C_{CENT}\times V_{CENT}\times k_{12}-C_{PER}\times V_{PER}\times k_{21} \quad (2)$$

$$dA_{GW}/dt = -(C_{GW}\times V_{GW}\times k_{PV})+C_{GL}\times V_{GL}\times k_{GL}- C_{GW}\times CL_{int,\,GW}\times C_{E(t),\,GW}/C_{E0} \quad (3)$$

$$dA_{PV}/dt = C_{GW}\times V_{GW}\times k_{PV} -Q_{PV}\times C_{PV} +Q_{PV}\times C_{CENT} \quad (4)$$

$$dA_{LIV}/dt = -(C_{LIV}\times f_u\times (CL_{int,3A}\times C_{E(t),\,LIV}/C_{E0}+CL_{int,non3A}))+Q_{PV}\times C_{PV}-Q_H\times C_{LIV}+ Q_{HA}\times C_{CENT} \quad (5)$$

DMD Fast Forward. Published on May 6, 2009 as DOI: 10.1124/dmd.109.026658
This article has not been copyedited and formatted. The final version may differ from this version.

where A_{CENT}, A_{PER}, A_{GW}, A_{PV}, and A_{LIV} are the amount of drug in central, peripheral, gut wall, portal vein, and liver compartment. C_{CENT}, C_{PER}, C_{GW}, $C_{GL,}$ C_{PV}, and C_{LIV} are drug concentrations and V_{CENT}, V_{PER}, V_{GL}, V_{GW}, V_{PV}, and V_{LIV} are the volume of central, peripheral, gut lumen, gut wall, portal vein, and liver compartment. V_{GW} is the same as the volume of water a patient would take to administer the drug, which is usually 250 mL. k_{GL} and k_{PV} are first order rate constant for drug transferring from gut lumen to gut wall and from gut wall to portal vein, respectively. k_{12} and k_{21} are the first order rate constants for drug transferring from central to peripheral and from peripheral to central compartments, respectively. $C_{E(t),GW}$ and $C_{E(t),LIV}$ are the concentration of active CYP3A in gut wall and liver at any time and C_{E0} is the baseline CYP3A concentration at time zero. $CL_{int,GW}$ and $CL_{int,3A}$ and $CL_{int,non3A}$ are intrinsic clearance in gut wall and the intrinsic clearance for CYP3A pathway and other metabolism pathway in the liver, respectively. CL_{REN} is renal clearance. f_u is fraction unbound in plasma. Q_H is the liver blood flow. Q_{PV} and Q_{HA} are the portal blood flow and hepatic artery blood flow and represent 75% and 25% of Q_H, respectively.

Equations 1-5 also applied for the inhibitor DTZ. Furthermore, a metabolite compartment was incorporated for the major metabolite of CYP3A4 pathway, nd-DTZ. The equations for nd-DTZ and the metabolites from other pathways (non-CYP3A4 pathway) are:

$$dA_{nd\text{-}DTZ}/dt = C_{LIV,DTZ} \times f_u \times CL_{int,3A} \times C_{E(t),LIV}/C_{E0} - C_{nd\text{-}DTZ} \times f_u \times CL_{nd\text{-}DTZ} \quad (6)$$

$$dA_{non3A}/dt = C_{LIV,DTZ} \times f_u \times CL_{int,non3A} \times C_{E(t),LIV}/C_{E0} - C_{non3A} \times f_u \times CL_{non3A} \quad (7)$$

where $A_{nd\text{-}DTZ}$, and $C_{nd\text{-}DTZ}$ are the amount and concentration of nd-DTZ formed, respectively. A_{non3A}, and C_{non3A} are the amount and concentration of metabolites formed from non-CYP3A4 pathway, respectively. $C_{LIV,DTZ}$ is DTZ concentration in liver. $CL_{int,3A}$ and $CL_{int,non3A}$ represent the intrinsic clearance of formation of nd-DTZ and other

DMD Fast Forward. Published on May 6, 2009 as DOI: 10.1124/dmd.109.026658
This article has not been copyedited and formatted. The final version may differ from this version.

metabolites, respectively. $CL_{nd\text{-}DTZ}$ and CL_{non3A} is the total clearance (including metabolic and renal clearance) of nd-DTZ and other metabolites, respectively.

Without inhibitors, the intrinsic clearance of MDZ in gut wall ($CL_{int,GW,MDZ}$, assuming only CYP3A in gut wall) and liver ($CL_{int,\ 3A,\ MDZ}$ and $CL_{int,\ non3A,\ MDZ}$) can be expressed in terms of $V_{max,GW,\ MDZ}$, $V_{max,3A,MDZ}$, $V_{max,non3A,\ MDZ}$, and $K_{m,MDZ}$,:

$$CL_{int,\,GW,\,MDZ} = \frac{V_{max,\,GW,\,MDZ}}{K_{m,\,MDZ} + C_{GW,\,MDZ}} \tag{8}$$

$$CL_{int,\,3A} = \frac{V_{max,\,3A,\,MDZ}}{K_{m,\,MDZ} + f_u \times C_{LIV,\,MDZ}}, CL_{int,\,non3A} = \frac{V_{max,\,non3A,\,MDZ}}{K_{m,\,MDZ} + f_u \times C_{LIV,\,MDZ}} \tag{9}$$

where $V_{max,GW,\ MDZ}$, $V_{max,3A,MDZ}$, $V_{max,non3A,\ MDZ}$, and $K_{m,MDZ}$ are the maximal rate for metabolite formation in gut wall, the maximal rate for metabolite formation through CYP3A4 and non-CYP3A4 pathway in liver, and the Michaelis-Menten constant, respectively, for MDZ. K_ms in the gut wall were assumed to be the same as those in the liver.

Following the administration of DTZ, the inactivator will produce a corresponding reduction in intrinsic clearance to CL'_{int}, as expressed in the following equations, considering DTZ and nd-DTZ act simultaneously as inhibitory species:

$$CL_{int,\,GW'} = \frac{V_{max,\,GW} \times \frac{E_{t,\,GW}}{E_0}}{K_m \times (1 + \frac{I_{t,\,GW,\,DTZ}}{K_{i,\,DTZ}}) + C_{GW}}, \quad CL_{int'} = \frac{V_{max,\,3A} \times \frac{E_{t,\,LIV}}{E_0} + V_{max,\,non3A}}{K_m(1 + \frac{I_{t,\,DTZ}}{K_{i,\,DTZ}} + \frac{I_{t,\,nd-DTZ}}{K_{i,\,nd-DTZ}}) + f_u \times C_{LIV}} \tag{10}$$

where $K_{i,DTZ}$ and $K_{i,nd\text{-}DTZ}$ are the competitive inhibition constant for DTZ and nd-DTZ, respectively. Note that nd-DTZ was considered to have no effect on gut wall CYP3A4 due to its minimal concentration in gut wall. Equations 8-10 also applied to the inhibitor, DTZ, because a change in the amount of active enzyme by the inhibitor, in turn, causes

DMD Fast Forward. Published on May 6, 2009 as DOI: 10.1124/dmd.109.026658
This article has not been copyedited and formatted. The final version may differ from this version.

a change in the intrinsic clearance and determine the nonlinear disposition of the inhibitor itself. We assume MDZ does nothing to DTZ or nd-DTZ.

The PK parameters for the development of MDZ PK model were estimated using a population approach, where the concentration-time data from 112 healthy subjects were combined from five clinical studies, as reported in a previous study by our group (Chien et al., 2006). The PK parameters are listed in Table 1 and were used for the simulation in the current study. The PK parameters for DTZ and nd-DTZ were obtained from data in the literature and listed in Table 2. Because the immediate-release (IR) preparation of DTZ is seldom used today, the disposition of the sustain-release (SR) preparation of DTZ and its interaction with MDZ were also simulated. The SR formulation of DTZ was modeled by modifying the k_{GL} from 0.9 (for IR formulation) to 0.2 and applying a lag time of four hours.

The enzyme model development

The amount of CYP3A4 in liver and gut wall was modeled as illustrated in Scheme 1. Panel A shows that at steady state without inactivator *in vivo*, the amount of active CYP3A4 enzyme (E_0) is determined by R_0, the rate of enzyme synthesis (zero order), and the rate of enzyme degradation, which is governed by the first order degradation rate constant, k_{deg}. In general, the rate of change of active enzyme ($E_{(t)}$) is given by:

$$\frac{dE_{(t)}}{dt} = R_0 - k_{deg} \times E_{(t)} \quad (11)$$

At baseline steady-state:

$$R_0 = k_{deg} \times E_0 \quad (12)$$

where E_0 is the amount of active enzyme at the time zero .

DMD Fast Forward. Published on May 6, 2009 as DOI: 10.1124/dmd.109.026658
This article has not been copyedited and formatted. The final version may differ from this version.

After the treatment with DTZ, assuming either DTZ or nd-DTZ acts as the inactivator, another pathway for enzyme inactivation is present, as depicted in Panel B. The rate of inactivation is determined by the pseudo-first order rate constant, k_{obs}.

$$\text{Rate of inactivation} = k_{obs} \times E_{(t)} = \frac{k_{inact} \times I_t}{K_I + I_t} \times E_{(t)} \quad (13)$$

where k_{inact} is the rate constant that defines the maximal rate of inactive enzyme formation, I_t is the inhibitor concentration at time t, and K_I is the inhibitor concentration when $k_{obs} = k_{inact}/2$. The differential equation for the amount of active CYP3A4 can then be expressed as following:

$$\frac{dE_{(t)}}{dt} = R_0 - k_{deg} \times E_{(t)} - \frac{k_{inact} \times I_t}{K_I + I_t} \times E_{(t)} \quad (14)$$

Panel C depicts the situation where both DTZ and nd-DTZ acted as CYP3A4 inactivators. An additive model was used for the simultaneous exposure to the two inactivators. The effect of competitive inhibition between the two inhibitors is also taken into account by incorporating a $(1+I_t/K_i)$ term into the model, as shown in the following equation:

$$\frac{dE_{(t)}}{dt} = k_{deg} \times E_0 - k_{deg} \times E_{(t)} - \left(\frac{k_{inact,\,DTZ} \times I_{t,\,DTZ}}{(1+\frac{I_{t,\,nd\text{ - }DTZ}}{K_{i,\,nd\text{ - }DTZ}}) \times K_{I,\,DTZ} + I_{t,\,DTZ}} + \frac{k_{inact,\,nd\text{ - }DTZ} \times I_{t,\,nd\text{ - }DTZ}}{(1+\frac{I_{t,\,DTZ}}{K_{i,\,DTZ}}) \times K_{I,\,nd\text{ - }DTZ} + I_{t,\,nd\text{ - }DTZ}} \right) \times E_{(t} \quad (15)$$

The reversible (K_i) and irreversible (k_{inact} and K_I) inhibition parameters were estimated for DTZ and nd-DTZ with human liver microsome (HLM) using a method as previously described (Jones et al., 1998). The values of the parameters were presented in a previous paper by our group, and are listed in Table 2 (Zhang et al., 2009). *In vivo* approaches estimate the half-life for CYP3A to be between 1 and 6 days (Zhang et al., 2008; Lai et al., 1978; Fromm et al., 1996; Hsu et al., 1997; Greenblatt et al., 2003). We

have examined the recovery of intestinal and hepatic CYP3A activity following a week-long course of clarithromycin (Gorski et al., 2002; Wang et al., 2004). By fitting the inactivation rate equation to the data, a half-life of CYP3A was determined to be approximately 28 hours ($k_{deg} \approx 0.03\ h^{-1}$). Therefore a k_{deg} value of 0.03 h^{-1} was used for the simulation in the current study (Table 2). Moreover, since the unbound fraction of DTZ in HLM is approximately 0.78 (Austin et al., 2002), a correction of K_I of DTZ by the unbound fraction in HLM was not made. The same was assumed for the metabolites of DTZ.

Model Validation and Prediction

The model was applied to simulate data of four sets of published data describing DTZ disposition (both IR and SR formulations) and DTZ IR/MDZ interaction studies (Table 3). Using the PK and enzyme inhibition parameters, Equations 1-15 were numerically solved to simulate the time course of the concentration of DTZ, nd-DTZ, MDZ, and the amount of active CYP3A4 in liver and gut wall, using the Pharsight Trial Simulator 2.2. (Pharsight Inc., Mountain View, CA).

The values of three key parameters (k_{inact}, K_I, and k_{deg}) were varied 10-fold within the simulation environment to quantify the sensitivity of the prediction of DTZ/MDZ interaction.

Clinical Study on DTZ/MDZ Interaction

Three healthy subjects (two males and one female) aged between 20 and 40 years were enrolled in a 2-phase, open-labeled, fixed-order study. All subjects gave written informed consent, and the study protocol was approved by the Institutional Review Board at Indiana University Purdue University Indianapolis.

Subjects were instructed to avoid taking any non-prescription or prescription medications and abstain from alcohol and grapefruit juice-containing products for one week prior to the start of the study and throughout the study. Subjects were excluded if

they were allergic to DTZ or MDZ; had clinically significant abnormalities in medical history, physical examination, routine serum chemistry, and urinalysis. Pregnant women as determined by a pregnancy test were excluded. On Phase 1 day 1, after an overnight fast, the subjects reported to the General Clinical Research Center. Intravenous catheters were placed in each forearm for the administration of drug and withdrawal of blood samples. Just prior to receiving the dose of MDZ, a baseline blood (5 ml) and a urine sample were obtained. MDZ (midazolam hydrochloride Injection, American Pharmaceutical Partners, Inc., Schaumburg, IL) 0.05mg/kg was infused intravenously at a constant rate over 30 minutes. Nine blood samples (6 ml each) were collected at baseline, 30 and 45 minutes and 1, 1.5, 2, 4, 8 and 12 hours after MDZ administration. On the morning of day 2, a 4 mg oral dose of MDZ hydrochloride syrup (Roxane Laboratory., Inc. Columbus, OH) was administered with 240 ml of tap water, and nine blood samples (6 ml each) were collected at 30 and 45 minutes and at 1, 1.5, 2, 4, 8, 12 and 24 hours following oral MDZ administration. The subjects began taking DTZ 120 mg twice daily for six days, and on the morning of day six after the initiation of DTZ treatment, the subjects returned to GCRC and Phase 2 began. IV and oral MDZ were given exactly the same as study day 1 and day 2 of Phase 1.

Serum concentrations of MDZ, DTZ, and nd-DTZ were measured using liquid chromatogram/mass spectrophotometry method as previously described (Pinto et al., 2005). PK parameters (C_{max}, T_{max}, $AUC_{0-\infty}$, and $T_{1/2}$) of MDZ before and after DTZ treatment were estimated by noncompartmental analysis using Winnonlin (ver 4.0; Pharsight, Mountain View, CA). A 2-tailed Student *t* test or Wilcoxon rank sum test, where appropriate, was performed to compare the pharmacokinetic parameter estimates before and after DTZ treatment. Differences were considered statistically significant at $p < .05$.

Results

Plasma Profiles of DTZ and nd-DTZ

Plasma concentration-time profiles of DTZ IR and SR, and nd-DTZ were simulated using the interaction model with the pharmacokinetic, physiological and enzyme kinetic parameters listed in Tables 1, and 2, and were compared with the reported data in literature. Figure 2A shows the concentration-time profiles of plasma DTZ after DTZ IR administrations at four different single oral doses (60 mg, 120 mg, 180 mg, and 210 mg). Overall, the simulated and reported profiles were comparable (Rovei et al., 1980). Moreover, the dose normalized $AUC_{0-\infty}$ (both observed and predicted) increased with the increase of dose, indicating nonlinear disposition, as shown in Figure 2B.

The predicted DTZ and nd-DTZ concentration profiles after the administration of a single dose of 90 mg DTZ IR are presented in Figure 3A and demonstrated good agreement with the observed data (Yeung et al., 1993). Shown in Figure 3B is the predicted and observed concentration-time profile of DTZ SR following the administration of DTZ SR 120 mg. The profile of SR was compared with IR at the same dose, and was predicted to have a longer T_{max} (~ 7 hrs), lower C_{max} (~ 80 mg/L), and slower terminal declining phase compared with the IR preparation. These simulated characteristics of DTZ SR were consistent with the observed data (Lefebvre et al, 1994). The above findings indicate the validity of the structure of the DTZ model and the parameters used in the present simulation for DTZ and nd-DTZ. The MDZ model was validated in a similar manner and have been presented elsewhere (Chien et al., 2006).

Effects of DTZ and nd-DTZ on Liver and Gut Wall CYP3A and MDZ AUC

The simulated DTZ and nd-DTZ concentration and their effects on the active CYP3A4 enzyme activity in the liver and gut wall following DTZ 60 mg bid for five doses are shown in Figure 4A and 4B. The observed DTZ concentration after the 4^{th} dose

agreed with the predicted DTZ profile (Backman et al., 1994). In response to DTZ administration, a maximum of 55% and 90% inactivation of liver and gut wall CYP3A4 was predicted, respectively (Fig. 4B). Furthermore, the decrease in the amount of CYP3A4 led to an increase in the AUC of MDZ by 3-fold when 15 mg MDZ was administered after DTZ treatment (Fig. 4C). This is consistent with the reported 3.75-fold increase (Backman et al., 1994).

Following administration of DTZ SR (120 mg twice daily for seven days), the plasma DTZ concentration was predicted to increase gradually and reach steady state in approximately two days with a maximal concentration at steady state of approximately 120 mg/L as shown in Figure 5A. The observed plasma DTZ concentration on day 1 and day 6 of DTZ administration showed excellent agreement with the predicted data (Lefebvre et al., 1994). On the other hand, the nd-DTZ concentration was predicted to decrease following repeated doses of DTZ and reached a plateau of 20 mg/L. This is probably due to the inactivation of CYP3A4 in liver, leading to a decreased formation rate of nd-DTZ. No observed data are available for nd-DTZ under this scenario. Furthermore, following DTZ administration, the active CYP3A4 in liver was predicted to fall gradually, and reach a plateau of approximately 40% of remaining activity. Upon the discontinuation of DTZ treatment, the activity recovered gradually, returning the original level in approximately five days. In contrast, gut wall CYP3A4 was predicted to decline almost immediately after the first dose of DTZ and reach a plateau of approximately 10% (Fig. 5B). We previously determined that a 38 ± 10% of the CYP3A4 activity remains in the gut wall under this dosing scenario (Fig. 5B). In our previous study, intestinal biopsies were obtained in ten healthy subjects after receiving DTZ (Cardizem SR®) 120 mg twice daily for seven days and ten healthy controls, and intestinal CYP3A4 activity was determined by incubating the small bowel tissue homogenate with MDZ *in vitro*.

DMD Fast Forward. Published on May 6, 2009 as DOI: 10.1124/dmd.109.026658
This article has not been copyedited and formatted. The final version may differ from this version.

The predicted profile of gut wall CYP3A4 activity using the PBPK model is consistent with the findings of the prior clinical study.

Clinical study on DTZ SR/MDZ interaction

Pharmacokinetic parameters of MDZ (mean ± SD) after administration of 4 mg of oral dose or 0.05 mg/kg of intravenous dose of MDZ before and after pretreatment of DTZ (Cardizem SR®, 120 mg twice daily) for six days to three volunteers are listed in Table 4. DTZ significantly increased the maximum serum concentration ($p < 0.05$) and the AUC ($p < 0.05$) of MDZ, without affecting the terminal half life or time to reach maximal serum concentration for both oral and iv MDZ. The mean fold increase of MDZ AUC was 4.1- and 1.6-fold for oral and iv MDZ, respectively.

Comparison of the effects of DTZ and nd-DTZ

The foregoing simulation results are based on the model where both DTZ and nd-DTZ (only affects liver CYP3A4) contribute to the overall inhibition effect following DTZ administration. The model was also used to simulate the remaining CYP3A4 activity in liver and gut wall, and the corresponding MDZ AUC increase supposing either DTZ or nd-DTZ acted as the inhibitory species in liver. As shown in figure 6A, the model predicted that DTZ or nd-DTZ alone caused approximately 45% maximal inactivation of liver CYP3A4 while a maximum of 60% inactivation of liver CYP3A4 was achieved if the effects of DTZ and nd-DTZ were both considered using the additive model. On the other hand, the gut wall CYP3A4 was the same under each situation because nd-DTZ did not reach the gut wall CYP3A4 in our model environment (Fig. 6B).

Correspondingly, the oral MDZ AUC was predicted to increase by 3.2-, 3.3-, and 4.2-fold; and the iv MDZ AUC was predicted to increase by 1.2-, 1.4-, and 1.6-fold when DTZ alone, nd-DTZ alone, or both were considered as inhibitors, respectively, for DTZ SR (Fig. 6C). Compared to the observed 4.1-fold increase of MDZ AUC as observed in the three patients, the model with both DTZ and nd-DTZ as inhibitors best predicted the

DTZ-MDZ interaction. The same holds true for DTZ IR administration as shown in Figure 6D.

Sensitivity Analysis

The sensitivity of the model prediction to the key model parameters was evaluated by varying individual parameters 5-fold from the value used for the prediction (an overall variation of 10-fold) using the model with DTZ as the inactivator as an example. For liver CYP3A4, a greater k_{inact} or a smaller K_I led to greater extent of CYP3A4 inactivation; while the greater the k_{deg}, the less the extent of CYP3A4 inactivation, and the faster the CYP3A4 was restored to its initial level (Fig. 7A, C, and E). As to CYP3A4 in gut wall, the overall pattern was similar to that of inactivation of liver CYP3A4, however, the effect of 10-fold variation in k_{inact}, K_I or k_{deg} on CYP3A4 level in gut wall was obscured due to extensive inactivation at this site (Fig. 7B, D, and F).

DMD Fast Forward. Published on May 6, 2009 as DOI: 10.1124/dmd.109.026658
This article has not been copyedited and formatted. The final version may differ from this version.

Discussion

The current study illustrated the development and validation of a semi-PBPK model for the prediction of the interaction between the mechanism-based inhibitor, DTZ, its major metabolite, nd-DTZ, and the prototypical CYP3A4 substrate, MDZ. The interaction model, takes into consideration the temporal change in inhibitor concentrations, gut wall interaction, and contribution from nd-DTZ, to successfully predicted the nonlinear disposition of DTZ and the interaction between DTZ and MDZ. The simulation results suggested that both DTZ and nd-DTZ contributed to the overall inhibitory effect observed following the administration of DTZ. The sensitivity analysis suggested that the *in vitro*-estimated enzyme inhibition parameters (k_{inact}, K_I, and K_i) and the CYP3A4 degradation rate constant, k_{deg}, are critical for the model prediction (Fig. 7).

Efforts have been made to predict *in vivo* DDIs involving mechanism-based inhibition with varying degrees of success and failure (Kanamitsu et al., 2000; Mayhew et al., 2000; Takanaga et al., 2000; Ito et al., 2003; Wang et al., 2004; Venkatakrishnan and Obach, 2005). The core interaction model used in these approaches considered the changes in the amount of active enzyme in the presence of a mechanism-based inhibitor, which in turn, determined the nonlinear elimination of inhibitors and the corresponding DDIs (Jones and Hall, 2002). Successful predictions have been reported for several mechanism-based inhibitors of CYP3A4. In the example of the MDZ/verapamil interaction, the intrinsic clearance of gut wall CYP3A4 was applied in an attempt to account for the gut wall metabolism, but only a single inhibitor concentration (the unbound average plasma concentration of the inhibitor at the steady state) was used in this study (Wang et al., 2004). The MDZ/macrolides, triazolam/ERY, and 5-fluorouracil/sorivudine interactions were successfully predicted using a semi-PBPK model, where the temporal change of inhibitors was adequately addressed (Kanamitsu et al., 2000; Ito et al., 2003). However, the gut wall metabolism and interaction was

accounted for in a relatively simplistic method by incorporating an F_g term (fraction of the dose that is metabolized in gut wall) with a fixed value. The results of current study indicate the importance of incorporating the temporal disposition of the inhibitor and DDIs at gut wall into the model development.

nd-DTZ has been shown to be more potent than its parent drug, as both reversible and irreversible inhibitor of CYP3A4 *in vitro* (K_i is 11-fold lower and k_{inact}/K_I is 4-fold higher than DTZ) (Sutton et al., 1997; Mayhew et al., 2000). Zhao et al. studied CYP3A4 inactivation by DTZ in human hepatocytes and suggested that the loss of CYP3A4 activity incubated with DTZ may be largely attributed to nd-DTZ (Zhao et al., 2007). However, the role of nd-DTZ *in vivo* remains unclear due to several factors. First, it is unlikely that nd-DTZ will be extensively excreted from the systemic circulation into the intestinal lumen and exert inhibitory effect on CYP3A4 in the enterocytes. Second, the level of nd-DTZ in systemic circulation is only about one-third of that of DTZ (Hermann and Morselli, 1985). In the current study, the model predicted that DTZ or nd-DTZ had similar effects on liver CYP3A4 activity (Fig. 6A) but neither DTZ nor nd-DTZ alone can fully account for the observed increase in MDZ AUC. Therefore, simulation with the drug and metabolite PBPK model provides a valuable tool for studying *in vivo* DDIs involving metabolites that would otherwise be difficult to identify. With the additive model incorporated into the semi-PBPK model for the simultaneous inactivation by DTZ and nd-DTZ, the fold increase of MDZ AUC following oral and intravenous administration was accurately predicted. The detailed evaluation of the additive model for the extent of inhibition in the presence of multiple inhibitors is presented in a previous study by our group (Zhang et al., 2009). One point needs to be clarified is that DTZ must be first metabolized to nd-DTZ to inactivate the enzyme. The inactivation parameters derived for DTZ will include the possibility that some nd-DTZ is formed but does not leave the active site but leads to the terminal inactivating species. Some nd-DTZ leaves the active

site and enters the systemic circulation such that equilibrium is reached between hepatic and systemic unbound concentrations. This metabolite will then re-enter the enzyme active site, after competing with DTZ, and inactivate with the intrinsic potency of the metabolite per se.

The expression of CYPs in enterocytes results in significant presystemic intestinal metabolism of drugs and possible gut wall DDIs following oral administration (Schwenk, 1988; Kaminsky and Fasco, 1991; Paine and Oberlies, 2007). The results of the current clinical study showed that DTZ treatment led to a much higher AUC increase for oral MDZ (4.1-fold) than iv MDZ (1.6-fold), suggesting the interaction between DTZ and MDZ occurred mainly during first-pass for this low extraction ratio drug. This conclusion was also supported by the observation that the terminal half life of MDZ was not affected by DTZ treatment. The prediction of DDIs at the level of the gut wall remains challenging due to the added uncertainty in the effective inhibitor concentration at this site. In the current model, drug concentration in gut wall is the amount of drug presented in the gut wall compartment in a volume of 250 mL, which is the volume of water a patient would take with the drug. Relatively high DTZ concentration was predicted in gut wall by this approach. When inhibitor concentration (It) is much higher than K_I, It in equation 1 is insignificant and inactivation occurrs at its maximal rate kinact. Although the gut wall concentration may not be identical to this value, it is undoubtedly high enough to result in k_{inact} condition. Thus it is the duration of exposure rather than the precise gut wall concentration that determines the extent and duration of the gut wall inhibition. This translated into a 10-20% remaining CY3A4 activity in gut wall at steady-state after DTZ treatment for six days, and effectively predicted the saturation in gut wall metabolism during first-pass elimination and the corresponding increase in MDZ AUC following oral administration. The enzyme parameters (k_{inact}, K_I, K_i, K_m, and V_{max}) for gut wall

CYP3A4 were assumed equivalent to that for liver CYP3A4 in the current study. This is supported by the evidence that although difference in V_{max} for liver and gut wall CYP3A4 has been reported when studied *in vitro*, once these data are normalized in terms of P450 expression level and method of isolation they are in fact very close (Galetin and Houston, 2006). However further studies on possible discrepancy in the intrinsic clearance and inhibition parameters of drugs for liver and gut wall enzymes are needed.

The CYP3A4 degradation rate constant, k_{deg} is of great importance for the prediction as shown by the sensitivity analysis where k_{deg} was shown to influence every stage of the CYP3A4 inactivation-recovery process (time to reach maximal inactivation, the extent of maximal inactivation, and time for recovery) (Fig. 7). However, k_{deg} is characterized by considerable uncertainty due to the difficulties estimating the value *in vivo*. A variety of approaches, including CYP3A turnover rate in CYP3A4-expressing Caco-2 cells (Malhotra S et al., 2001), primary human hepatocytes (Pichard et al., 1992); liver slices (Renwick et al., 2000), or rats (Correia, 1991); time course of recovery of CYP3A4 activity following inactivation by grape fruit juice *in vivo* (Greenblatt et al., 2003); time course of de-induction of rifampin and carbamazepine *in* vivo (Lai et al., 1978; Fromm et al., 1996); and auto-induction following ritonavir *in vivo* (Hsu et al., 1997) have been applied in an attempt to obtain an accurate estimate of this parameter. The values for k_{deg} estimated with these approaches vary from 0.005 to 0.07 hr^{-1}. A value of 0.03 hr^{-1} was used for k_{deg} in both liver and gut wall in the current study based on a clinical study by our group where MDZ/clarithromycin data were fitted into the inactivation model (in press). This value is also consistent with the previous estimate for the intestinal CYP3A4 (Greenblatt et al., 2003).

Studies have suggested that the uptake and efflux transporters in liver or gut wall might play important roles in the disposition of many compounds but the effect of

transporters was not incorporated in the current model development (Faber et al., 2003). MDZ is not transported at gut wall or liver (Franke et al., 2008). DTZ has been identified as a p-gp substrate (Katoh et al., 2006), but because it is highly water soluble (solubility in water is 56.6g/100mL) and highly lipophilic (log P = 2.3), transport is not expected to be an important modulator of intracellular concentration. Therefore, metabolism, not liver or gut uptake is likely to be the rate-limiting step of the overall disposition of DTZ. Nevertheless, drug transporter effects should be considered in future modeling and simulation studies, especially for the many class 3 drugs (high solubility, low permeability with elimination primarily as unchanged drug in humans) for which gut or hepatic uptake could limit their disposition.

In summary, the clinical study indicated that DTZ administration significantly elevated MDZ exposure following oral but not intravenous administration, suggesting DDIs in gut wall plays an important role in the interaction between DTZ and MDZ. The semi-PBPK model incorporating DDIs at gut wall and the effect of nd-DTZ successfully predicted nonlinear disposition of DTZ and its interaction with MDZ. Furthermore, model simulation suggested both DTZ and nd-DTZ contributed to the overall inhibitory effect following DTZ administration and the values of the *in vitro* estimated inhibition parameters and CYP3A4 turnover rate are critical for the prediction.

Acknowledgement

The authors would like to acknowledge Dr. Aroonrut Lucksiri for her contribution to this manuscript.

References

Austin RP, Barton P, Cockroft SL, Wenlock MC, and Riley RJ (2002) The influence of nonspecific microsomal binding on apparent intrinsic clearance, and its prediction from physicochemical properties. Drug Metab Dispos. **30**:1497-503.

Azie NE, Brater DC, Becker PA, Jones DR and Hall SD (1998) The interaction of diltiazem with lovastatin and pravastatin. Clin Pharmacol Ther **64**:369-377.

Backman JT, Olkkola KT, Aranko K, Himberg JJ and Neuvonen PJ (1994) Dose of midazolam should be reduced during diltiazem and verapamil treatments. Br J Clin Pharmacol **37**:221-225.

Bianchetti G, Regazzi M, Rondanelli R, Ascalone V and Morselli PL (1991) Bioavailability of diltiazem as a function of the administered dose. Biopharm Drug Dispos **12**:391-401.

Brodie MJ and MacPhee GJ (1986) Carbamazepine neurotoxicity precipitated by diltiazem. Br Med J (Clin Res Ed) **292**:1170-1171.

Brown JM, Quedens-Case C, Alderman JL, Greener Y, Taylor KJ (1997) Contrast enhanced sonography of visceral perfusion defects in dogs. J Ultrasound Med. **16**:493-9.

Buckley MM, Grant SM, Goa KL, McTavish D and Sorkin EM (1990) Diltiazem. A reappraisal of its pharmacological properties and therapeutic use. Drugs **39**:757-806.

Chaffman M and Brogden RN (1985) Diltiazem. A review of its pharmacological properties and therapeutic efficacy. Drugs **29**:387-454.

Chien JY, Lucksiri A, Ernest CS, 2nd, Gorski JC, Wrighton SA and Hall SD (2006) Stochastic prediction of CYP3A-mediated inhibition of midazolam clearance by ketoconazole. Drug Metab Dispos **34**:1208-1219.

Correia MA (1991) Cytochrome P450 turnover. Methods Enzymol **206**:315-325.

Eimer M and Carter BL (1987) Elevated serum carbamazepine concentrations following diltiazem initiation. Drug Intell Clin Pharm **21**:340-342.

Faber KN, Muller M and Jansen PL (2003) Drug transport proteins in the liver. Adv Drug Deliv Rev **55**:107-124.

Franke RM, Baker SD, Mathijssen RH, Schuetz EG, and Sparreboom A. (2008) Influence of solute carriers on the pharmacokinetics of CYP3A4 probes. Clin Pharmacol Ther 84:704-9.

Fromm MF, Kroemer HK, and Eichelbaum M. (1996) Differential induction of prehepatic and hepatic metabolism of verapamil by rifampin. Hepatology **24**:796-801.

Galetin A and Houston JB (2006) Intestinal and hepatic metabolic activity of five cytochrome P450 enzymes: impact on prediction of first-pass metabolism. . Pharmacol Exp Ther. **318**:1220-9.

Gorski JC, Wang Z and Hall SD (2002) Duration of CYP3A inhibition by clarithromycin. Clinl Pharmacol Ther **71**:MPI-105.

Greenblatt DJ, von Moltke LL, Harmatz JS, Chen G, Weemhoff JL, Jen C, Kelley CJ, LeDuc BW and Zinny MA (2003) Time course of recovery of cytochrome p450 3A function after single doses of grapefruit juice. Clin Pharmacol Ther **74:**121-129.

Hermann P and Morselli PL (1985) Pharmacokinetics of diltiazem and other calcium entry blockers. *Acta Pharmacol Toxicol (Copenh)* **57 Suppl 2:**10-20.

Hermann P RS, Remones G, Thenot JP, London DR, Morselli PL. (1983) Pharmacokinetics of diltiazem after intravenous and oral administration. *Eur J Clin Pharmacol* **24:**349-352.

Hoglund P and Nilsson LG (1989) Pharmacokinetics of diltiazem and its metabolites after repeated single dosing in healthy volunteers. *Ther Drug Monit* **11:**551-557.

Hsu A, Granneman GR, Witt G, Locke C, Denissen J, Molla A, Valdes J, Smith J, Erdman K, Lyons N, Niu P, Decourt JP, Fourtillan JB, Girault J and Leonard JM (1997) Multiple-dose pharmacokinetics of ritonavir in human immunodeficiency virus-infected subjects. *Antimicrob Agents Chemother* **41:**898-905.

Ito K, Ogihara K, Kanamitsu S and Itoh T (2003) Prediction of the in vivo interaction between midazolam and macrolides based on in vitro studies using human liver microsomes. *Drug Metab Dispos* **31:**945-954.

Jones DR and Hall SD (2002) Mechanism-based inhibition of human cytochromes P450: in vitro kinetics and in vitro-in vivo correlations. Marcel Dekker, Inc, New York.

Jones DR, Gorski JC, Hamman MA, Mayhew BS, Rider S and Hall SD (1999) Diltiazem inhibition of cytochrome P-450 3A activity is due to metabolite intermediate complex formation. *J Pharmacol Exp Ther* **290:**1116-1125.

Kaminsky LS and Fasco MJ (1991) Small intestinal cytochromes P450. *Crit Rev Toxicol* **21:**407-422.

Kanamitsu SI, Ito K, Okuda H, Ogura K, Watabe T, Muro K and Sugiyama Y (2000) Prediction of in vivo drug-drug interactions based on mechanism-based inhibition from in vitro data: inhibition of 5-fluorouracil metabolism by (E)-5-(2-Bromovinyl)uracil. *Drug Metab Dispos* **28:**467-474.

Katoh M, Suzuyama N, Takeuchi T, Yoshitomi S, Asahi S, and Yokoi T (2006) Kinetics analysis for species differences in P-glycoprotein-mediated drug transport. J Pharm Sci. **95**:2673-83.

Lai AA, Levy RH and Cutler RE (1978) Time-course of interaction between carbamazepine and clonazepam in normal man. *Clin Pharmacol Ther* **24:**316-323.

Lefebvre M LY, Spenard J, Geadah D, Moisan R, Gossard D, Landriault H, Du Souich P, Caille G (1994) Pharmacokinetics and pharmacodynamics of a slow-release

formulation of diltiazem after the administration of a single and repeated doses to healthy volunteers. *Biopharm drug dipos* **15:**227-242.

Malhotra S, Schimiedlin-Ren P, Paine MF, Criss AB and P W (2001) The furocoumarin 6', 7'-dihydroxybergamottin (DHB) accelarates CYP3A4 degradation via the ubiquitin-proteasomal pathway. *Drug Metab Rev* **33:**97.

Masica AL, Azie NE, Brater DC, Hall SD and Jones DR (2000) Intravenous diltiazem and CYP3A-mediated metabolism. *Br J Clin Pharmacol* **50:**273-276.

Mayhew BS, Jones DR and Hall SD (2000) An in vitro model for predicting in vivo inhibition of cytochrome P450 3A4 by metabolic intermediate complex formation. *Drug Metab Dispos* **28:**1031-1037.

Paine MF and Oberlies NH (2007) Clinical relevance of the small intestine as an organ of drug elimination: drug-fruit juice interactions. *Expert Opin Drug Metab Toxicol* **3:**67-80.

Pichard L, Fabre I, Daujat M, Domergue J, Joyeux H and Maurel P (1992) Effect of corticosteroids on the expression of cytochromes P450 and on cyclosporin A oxidase activity in primary cultures of human hepatocytes. *Mol Pharmacol.* **41:**1047-1055.

Piepho RW, Bloedow DC, Lacz JP, Runser DJ, Dimmit DC and Browne RK (1982) Pharmacokinetics of diltiazem in selected animal species and human beings. *Am J Cardiol* **49:**525-528.

Pinto AG, Horlander J, Chalasani N, Hamman M, Asghar A, Kolwankar D and Hall SD (2005) Diltiazem inhibits human intestinal cytochrome P450 3A (CYP3A) activity in vivo without altering the expression of intestinal mRNA or protein. *Br J Clin Pharmacol* **59:**440-446.

Renwick AB, Watts PS, Edwards RJ, Barton PT, Guyonnet I, Price RJ, Tredger JM, Pelkonen O, Boobis AR and Lake BG (2000) Differential maintenance of

cytochrome P450 enzymes in cultured precision-cut human liver slices. *Drug Metab Dispos* **28:**1202-1209.

Rovei V, Gomeni R, Mitchard M, Larribaud J, Blatrix C, Thebault JJ and Morselli PL (1980) Pharmacokinetics and metabolism of diltiazem in man. *Acta Cardiol* **35:**35-45.

Schwenk M (1988) Mucosal biotransformation. *Toxicol Pathol* **16:**138-146.

Smith MS, Verghese CP, Shand DG and Pritchett EL (1983) Pharmacokinetic and pharmacodynamic effects of diltiazem. *Am J Cardiol* **51:**1369-1374.

Sutton D, Butler AM, Nadin L and Murray M (1997) Role of CYP3A4 in human hepatic diltiazem N-demethylation: inhibition of CYP3A4 activity by oxidized diltiazem metabolites. *J Pharmacol Exp Ther* **282:**294-300.

Takanaga H, Ohnishi A, Matsuo H, Murakami H, Sata H, Kuroda K, Urae A, Higuchi S and Sawada Y (2000) Pharmacokinetic analysis of felodipine-grapefruit juice interaction based on an irreversible enzyme inhibition model. *Br J Clin Pharmacol* **49:**49-58.

Varhe A, Olkkola KT and Neuvonen PJ (1996) Diltiazem enhances the effects of triazolam by inhibiting its metabolism. *Clin Pharmacol Ther* **59:**369-375.

Venkatakrishnan K and Obach RS (2005) In vitro-in vivo extrapolation of CYP2D6 inactivation by paroxetine: prediction of nonstationary pharmacokinetics and drug interaction magnitude. *Drug Metab Dispos* **33:**845-852.

Wagner K, Henkel M, Heinemeyer G and Neumayer HH (1988) Interaction of calcium blockers and cyclosporine. *Transplant Proc* **20:**561-568.

Wang YH, Jones DR and Hall SD (2004) Prediction of cytochrome P450 3A inhibition by verapamil enantiomers and their metabolites. *Drug Metab Dispos* **32:**259-266.

Yeung PK, Prescott C, Haddad C, Montague TJ, McGregor C, Quilliam MA, Xei M, Li R, Farmer P and Klassen GA (1993) Pharmacokinetics and metabolism of diltiazem

in healthy males and females following a single oral dose. *Eur J Drug Metab Pharmacokinet* **18:**199-206.

Zelis RF and Kinney EL (1982) The pharmacokinetics of diltiazem in healthy American men. *Am J Cardiol* **49:**529-532.

Zhang X, Jones, DR and Hall SD (2009) Prediction of the effect of erythromycin, diltiazem, and their metabolites, alone and in combination, on CYP3A4 inhibition. *Drug Metab Dispos* **37**:150-60.

Zhang X, Jones DR, and Hall SD (2008). Mechanism-based inhibition of human cytochromes P450: *in vitro* kinetics and *in vitro-in vivo* correlations. In: Drug-drug Interactions, Second Edition. Ed. Rodrigues AS. Marcel Dekker, New York, NY.

Zhao P, Lee CA and Kunze KL (2007) Sequential metabolism is responsible for diltiazem induced time-dependent loss of CYP3A. *Drug Metab Dispos* **35**:704-12.

Footnotes

[1] current affiliation: Department of Drug Disposition, Eli Lilly and Company, Indianapolis, IN

[2] current affiliation: Division of Biostatistics, Indiana University School of Medicine, Indianapolis, IN

[3] current affiliation: Mylan Pharmaceuticals, Inc., Morgantown, WV

Figure legends

Figure 1. Semi-PBPK model for the description of the disposition of DTZ and MDZ.

Figure 2. Predicted and observed concentration-time profile (A) and dose-normalized $AUC_{0-\infty}$ (B) for DTZ following increasing single oral doses.
In A, the lines are predicted concentration profiles using the semi-PBPK model. The symbols are observed concentration profiles following 60 mg (●), 120 mg (▲), 180 mg (■), and 210 mg (♦) dose of DTZ (Rovei et al., 1980).

Figure 3. Predicted and observed concentration-time profiles for DTZ and nd-DTZ following a single oral dose of 60 mg of DTZ immediate-release formulation (A), and for DTZ following a single oral dose of 120 mg of DTZ immediate-release formulation and DTZ sustained-release formulation (B). The circles are the corresponding observed data (Yeung et al., 1993; Lefevbre et al., 1994)

Figure 4. Predicted concentrations of DTZ and nd-DTZ (A), active CYP3A4 content in liver (solid line) and gut wall (dashed line) (B), and MDZ AUC increase (C) following DTZ immediate-release formulation 60 mg three times a day for five doses. The closed circles in panel A are observed DTZ concentration after the fourth dose of DTZ (Backman et al., 1994). In panel C, MDZ 10 mg was given orally before and after the fourth dose of DTZ.

Figure 5. Predicted and observed concentration profiles of DTZ (solid line) and nd-DTZ (dashed line) (A), and active CYP3A4 in liver (solid line) and gut wall (dashed line) (B) following DTZ sustained-release formulation 120 mg twice a day for seven days. The

closed circles in panel A are observed DTZ concentrations on day 1 and day 6 of DTZ treatment (Lefebvre et al., 1994). The close circle with error bar in panel B is observed CYP3A4 activity on the morning of the 8^{th} day (Pinto et al., 2005).

Figure 6. Simulated percentage of the remaining CYP3A4 activity in liver (A) and gut wall (B) with DTZ alone (dashed lines), nd-DTZ alone (solid lines), and DTZ + nd-DTZ (dash-dot lines) as inhibitors, and comparison between observed MDZ AUC fold increases and predicted MDZ AUC fold increases with DTZ alone, nd-DTZ alone, and DTZ + nd-DTZ as inhibitors following DTZ sustained-release formulation (C) and DTZ immediate-release formulation (D) treatments for oral and intravenous MDZ administration.

Figure 7. Effects of model parameters, k_{inact} (A and B), K_I (C and D), and k_{deg} (E and F), on the time course of percentage of the remaining enzyme activity in liver (A, C, and E) and gut wall (B, D, and F) during and after DTZ sustained-release formulation administration. The values of each parameter was varied 5-fold from that used in the prediction in this study.

DMD Fast Forward. Published on May 6, 2009 as DOI: 10.1124/dmd.109.026658
This article has not been copyedited and formatted. The final version may differ from this version.

Table 1. Model parameters for MDZ used in the simulations

Parameter	Values[a]
K_a (h^{-1})	1.2
V_c (L)	42.9
V_p (L)	88.4
CL_r (L/h)	0.06
CLint $_{3A}$ (L/h)	439
CLint $_{non3A}$ (L/h)	36
$V_{max, 3A}$ (mg/h)[b]	2549
$V_{max, non3A}$(mg/h)[b]	254
$V_{max, gw,3A}$(mg/h)[b]	2549
K_m (mg/L)[b]	5.8
f_u	0.04
V_{gw} (L)	0.25
V_{pv} (L)	0.07
V_{liv} (L)	2.8

[a] Adapted from Chien et al., 2006.

[b] K_m was estimated using human liver microsome in house. $V_{max,3A}$ was estimated by CLint $_{3A}$ x K_m. $V_{max, non3A}$ was estimated as approximately one tenth of $V_{max, 3A}$. $V_{max,gw,3A}$ was assumed the same as $V_{max,3A}$.

DMD Fast Forward. Published on May 6, 2009 as DOI: 10.1124/dmd.109.026658
This article has not been copyedited and formatted. The final version may differ from this version.

Table 2. Model parameters for DTZ and nd-DTZ.

Parameters		Values	References
PK parameters			
DTZ	K_a (h^{-1})	0.9	(Hermann P, 1983)
	T_{lag} (h)	0.5	(Hermann P, 1983)
	V_c (L)	120	(Hermann P, 1983)
	V_p (L)	141	(Hermann P, 1983)
	CL_r (L/h)	0.06	(Hermann P, 1983)
	CLint (L/h)	900	(Hermann P, 1983)
	$CLint_{3A}$ (L/h)	360 [a]	
	$CLint_{non3A}$ (L/h)	540	
	$V_{max, 3A}$ (mg/h)	432	
	$V_{max, non3A}$ (mg/h)	648	
	$V_{max, gw}$ (mg/h)	432	
	K_m (mg/L)	1.2	(Jones et al., 1999)
	f_u	0.2	(Piepho et al., 1982)
nd-DTZ	V_{nd-DTZ} (L)	261 [b]	
	$_{1/2}$ (h)	5	(Hoglund and Nilsson, 1989)
	CL_{nd-DTZ} (L)	36 [c]	
	f_u	0.2 [b]	
Physiological parameters			
	V_{gw} (L)	0.25	(Chien et al., 2006)
	V_{pv} (L)	0.07	(Ito et al., 2003)
	V_{liv} (L)	2.8	(Ito et al., 2003)
	k_{deg} (hr^{-1})	0.03	(Greenblatt et al., 2003)
Enzyme inhibition parameters [d]			
DTZ	K_i (uM)	41	
	k_{inact} (h^{-1})	4.2	
	K_I (uM)	3	
nd-DTZ	K_i (uM)	0.8	
	k_{inact} (h^{-1})	3	
	K_I (uM)	0.3	

[a]: assume CYP3A pathway accounts for one thirds of the total metabolic clearance
[b]: assume the same as that of DTZ
[c]: calculated from $V_{nd-DTZ} \times k_{el}$
[d]: estimated *in vitro* using HLM, see Materials and Methods

DMD Fast Forward. Published on May 6, 2009 as DOI: 10.1124/dmd.109.026658
This article has not been copyedited and formatted. The final version may differ from this version.

Table 3. Simulation scenarios used in the study.

Simulation scenario	References
DTZ IR 60 mg, po, single dose	(Hermann P, 1983)
DTZ IR 60 mg, for five doses	(Backman et al., 1994)
DTZ IR 60 mg, for 5 doses, MDZ 3.5 mg, iv infusion over two minutes, before DTZ administration and after the last dose of DTZ	N.A.
DTZ IR 60 mg, for five doses, MDZ 15 mg, po, before DTZ administration and after the last dose of DTZ	(Backman et al., 1994)
DTZ SR (Cardizem SR) 120 mg po, single oral dose	(Lefebvre , 1994)
DTZ SR (Cardizem SR) 120 mg po, twice daily for six days	(Lefebvre , 1994)
DTZ SR (Cardizem SR) 120 mg po, twice daily for six days, MDZ 0.05 mg/kg, iv infusion over two minutes, before and on day 6 of DTZ administration	Clinical study
DTZ SR (Cardizem SR) 120 mg po, twice daily for 6 days, MDZ 4 mg, po, before and on day 6 of DTZ administration	Clinical study

N.A.: not available.

DMD Fast Forward. Published on May 6, 2009 as DOI: 10.1124/dmd.109.026658
This article has not been copyedited and formatted. The final version may differ from this version.

Table 4 Pharmacokinetic parameters of MDZ (mean ± SD) after administration of 4 mg of oral dose or 0.05 mg/kg of intravenous dose of MDZ before and after pretreatment of DTZ SR (Cardizem SR, 120 mg twice daily) for seven days to three volunteers

	Oral MDZ			Intravenous MDZ		
	Before	After	*p* value	Before	After	*p* value
C_{max} (□g/L)	15.8 ± 2.8	41.3 ± 14.0	<0.05	87.3 ± 6.1	112.7 ± 9.0	<0.05
T_{max} (h)	1.3 ± 0.7	1.9 ± 0.2	0.18	0.5	0.5	N.A.
$AUC_{0-\infty}$ (□g*h/L)	69 ± 15.7	276.7 ± 33.3	<0.05	216.3 ± 58.5	372.0 ± 58.0	<0.05
$t_{1/2}$ (h)	6.0 ± 1.7	8.0 ±0.8	0.23	2.7 ± 0.7	4.1 ± 0.62	0.13

N.A.: not applicable.

DMD Fast Forward. Published on May 6, 2009 as DOI: 10.1124/dmd.109.026658
This article has not been copyedited and formatted. The final version may differ from this version.

Scheme 1

A

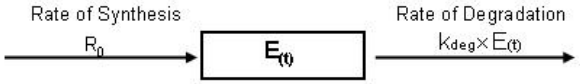

B

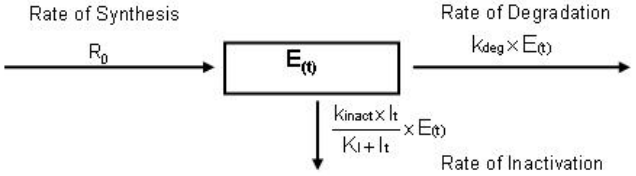

C

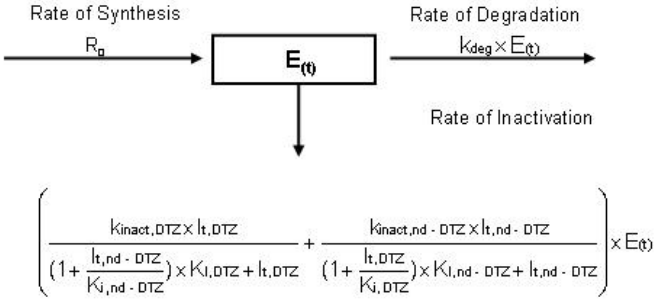

Fig. 1

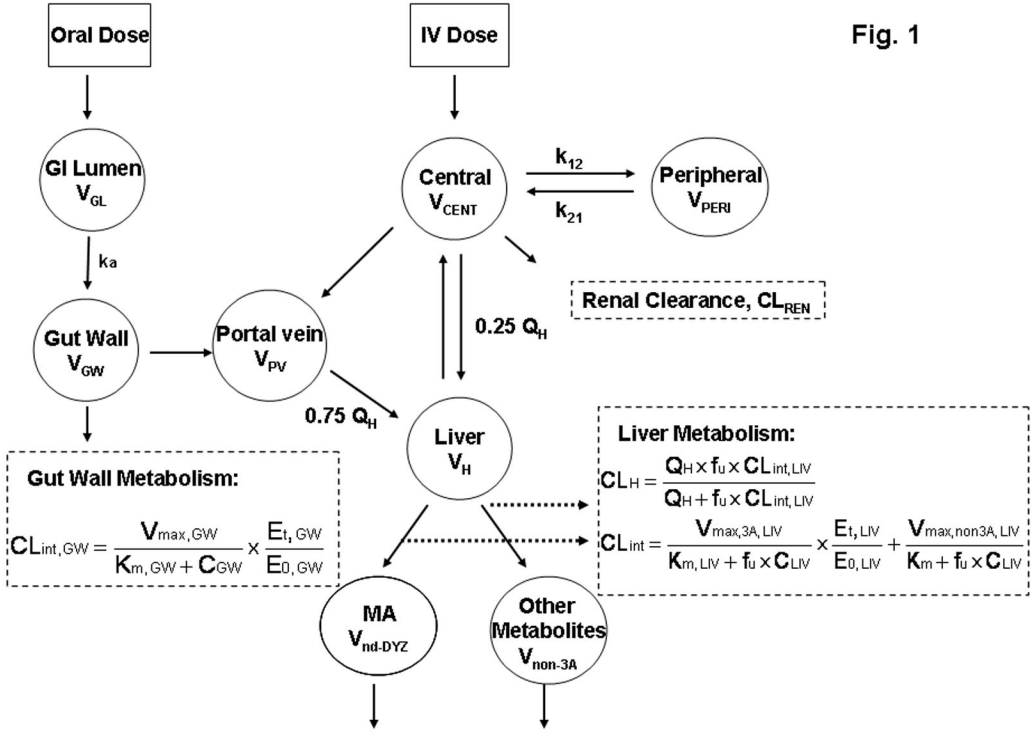
Oral Dose
IV Dose
GI Lumen
V_{GL}
ka
Central
V_{CENT}
k_{12}
k_{21}
Peripheral
V_{PERI}
Renal Clearance, CL_{REN}
Gut Wall
V_{GW}
Portal vein
V_{PV}
0.25 Q_H
0.75 Q_H
Liver
V_H
Gut Wall Metabolism:
$CL_{int,GW} = \frac{V_{max,GW}}{K_{m,GW} + C_{GW}} \times \frac{E_{t,GW}}{E_{0,GW}}$
Liver Metabolism:
$CL_H = \frac{Q_H \times f_u \times CL_{int,LIV}}{Q_H + f_u \times CL_{int,LIV}}$
$CL_{int} = \frac{V_{max,3A,LIV}}{K_{m,LIV} + f_u \times C_{LIV}} \times \frac{E_{t,LIV}}{E_{0,LIV}} + \frac{V_{max,non3A,LIV}}{K_m + f_u \times C_{LIV}}$
MA
V_{nd-DYZ}
Other Metabolites
V_{non-3A}

Fig2

A

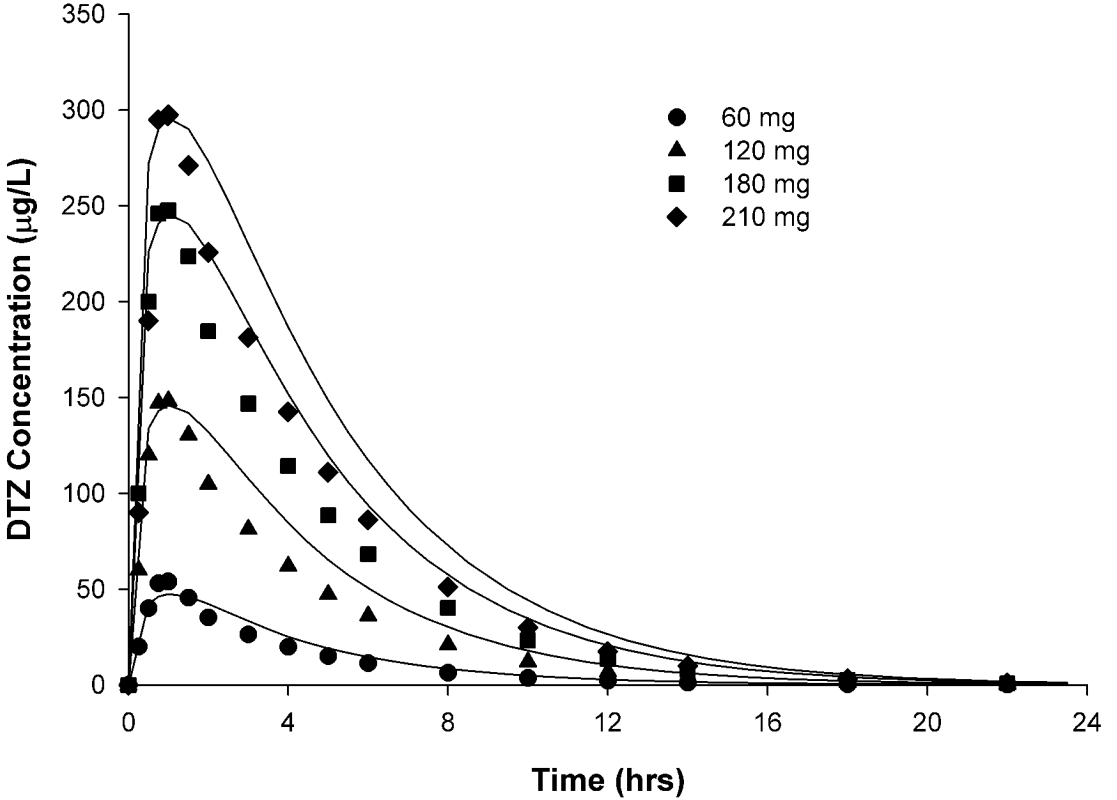
350
300
250
200
150
100
50
0
DTZ Concentration (μg/L)
0
4
8
12
16
20
24
Time (hrs)
60 mg
120 mg
180 mg
210 mg

DMD Fast Forward. Published on May 6, 2009 as DOI: 10.1124/dmd.109.026658
This article has not been copyedited and formatted. The final version may differ from this version.

Fig 2

B

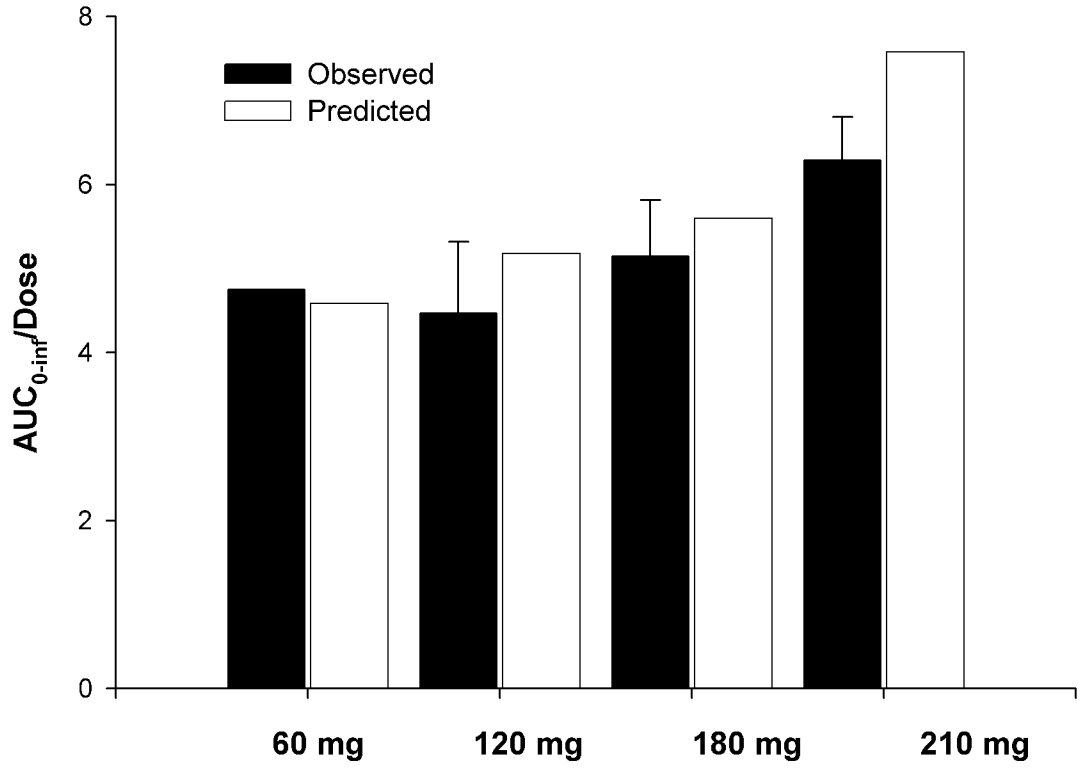

DMD Fast Forward. Published on May 6, 2009 as DOI: 10.1124/dmd.109.026658
This article has not been copyedited and formatted. The final version may differ from this version.

Fig 3

A

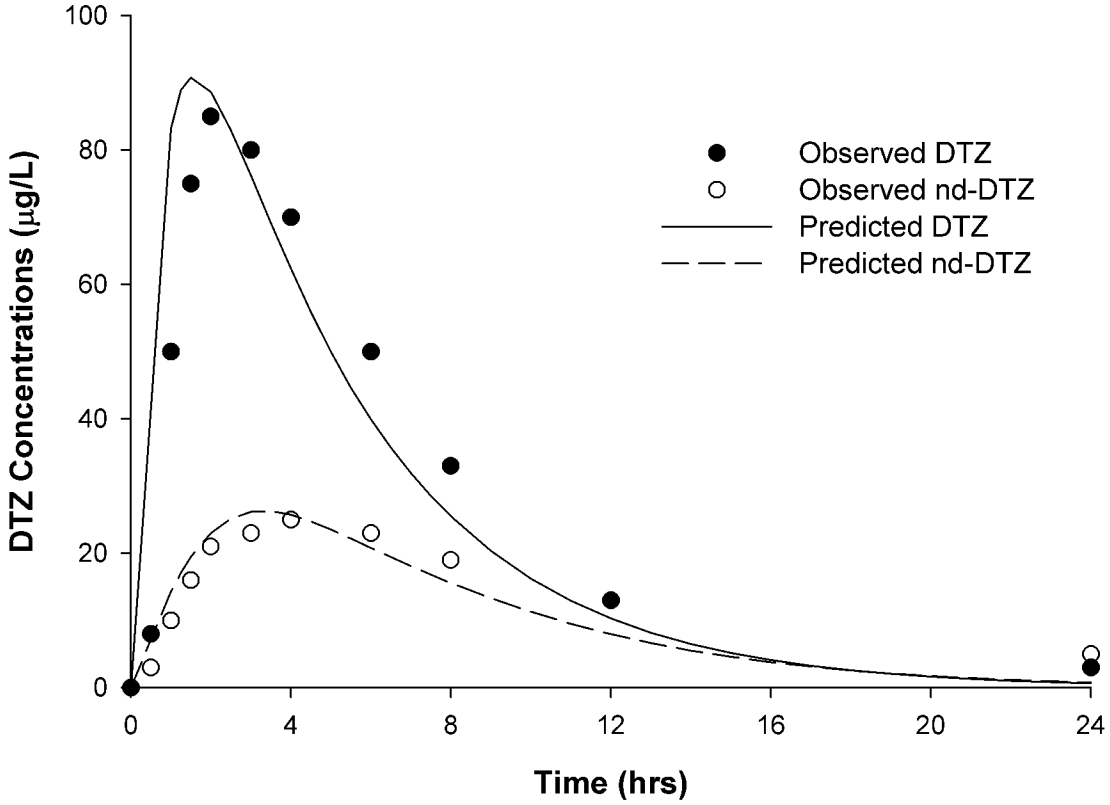

B

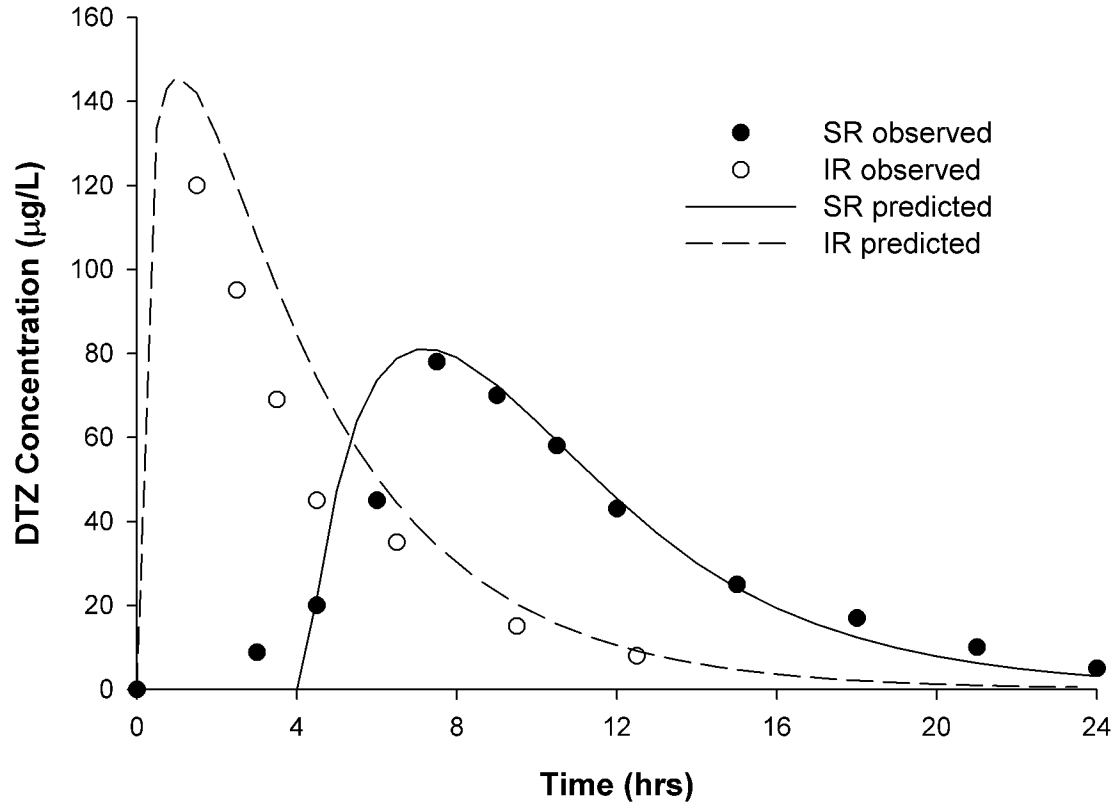

DMD Fast Forward. Published on May 6, 2009 as DOI: 10.1124/dmd.109.026658
This article has not been copyedited and formatted. The final version may differ from this version.

Fig 4

A

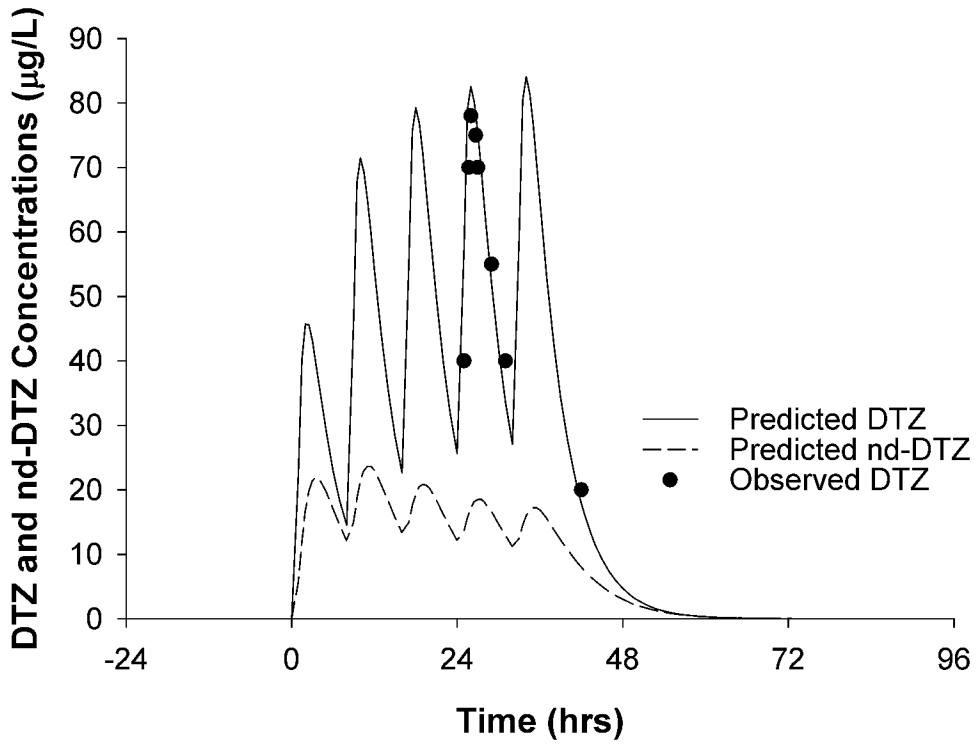

B

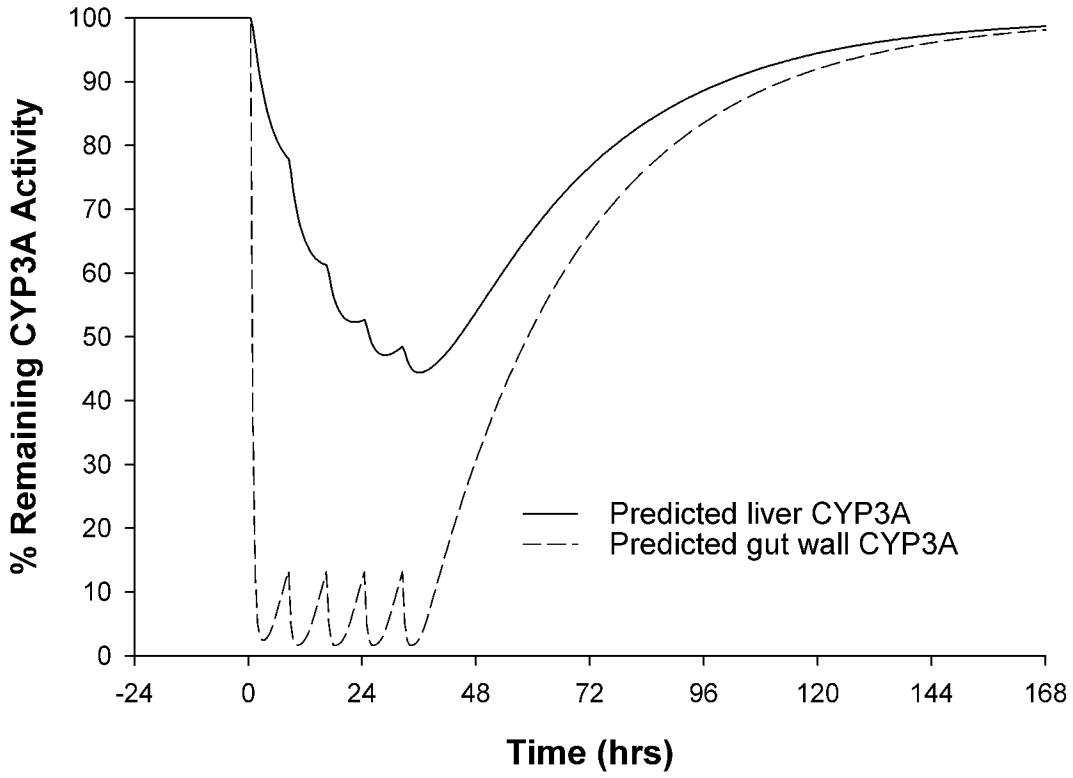

DMD Fast Forward. Published on May 6, 2009 as DOI: 10.1124/dmd.109.026658
This article has not been copyedited and formatted. The final version may differ from this version.

Fig 4

C

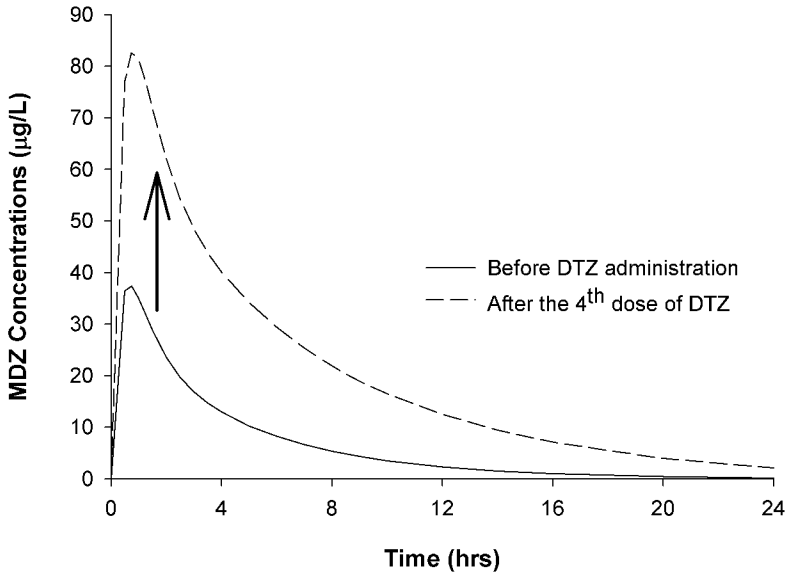

DMD Fast Forward. Published on May 6, 2009 as DOI: 10.1124/dmd.109.026658
This article has not been copyedited and formatted. The final version may differ from this version.

Fig 5

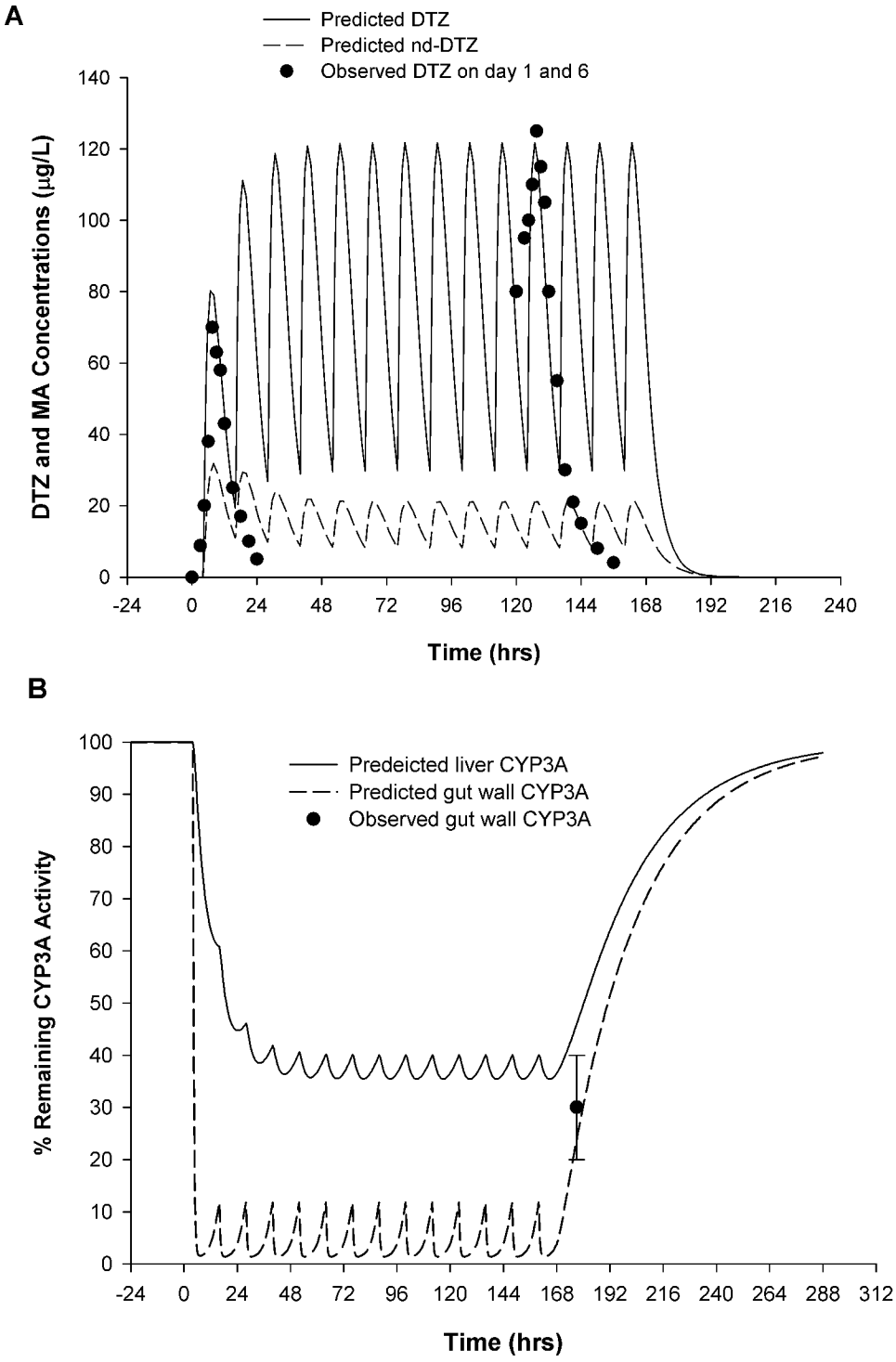

Fig 6

A

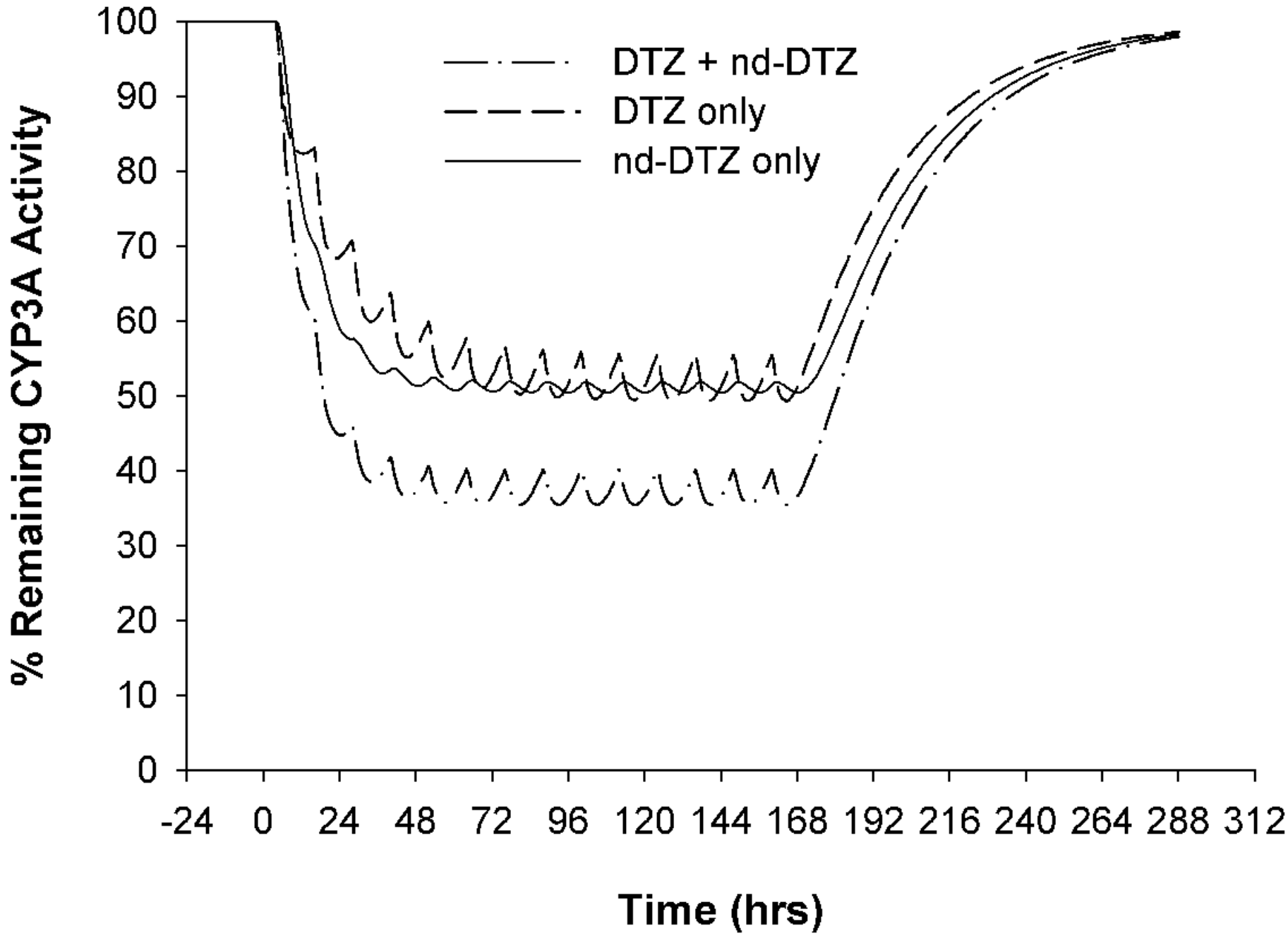
100
90
80
70
60
50
40
30
20
10
0
% Remaining CYP3A Activity
DTZ + nd-DTZ
DTZ only
nd-DTZ only
-24
0
24
48
72
96
120
144
168
192
216
240
264
288
312
Time (hrs)

Fig 6

B

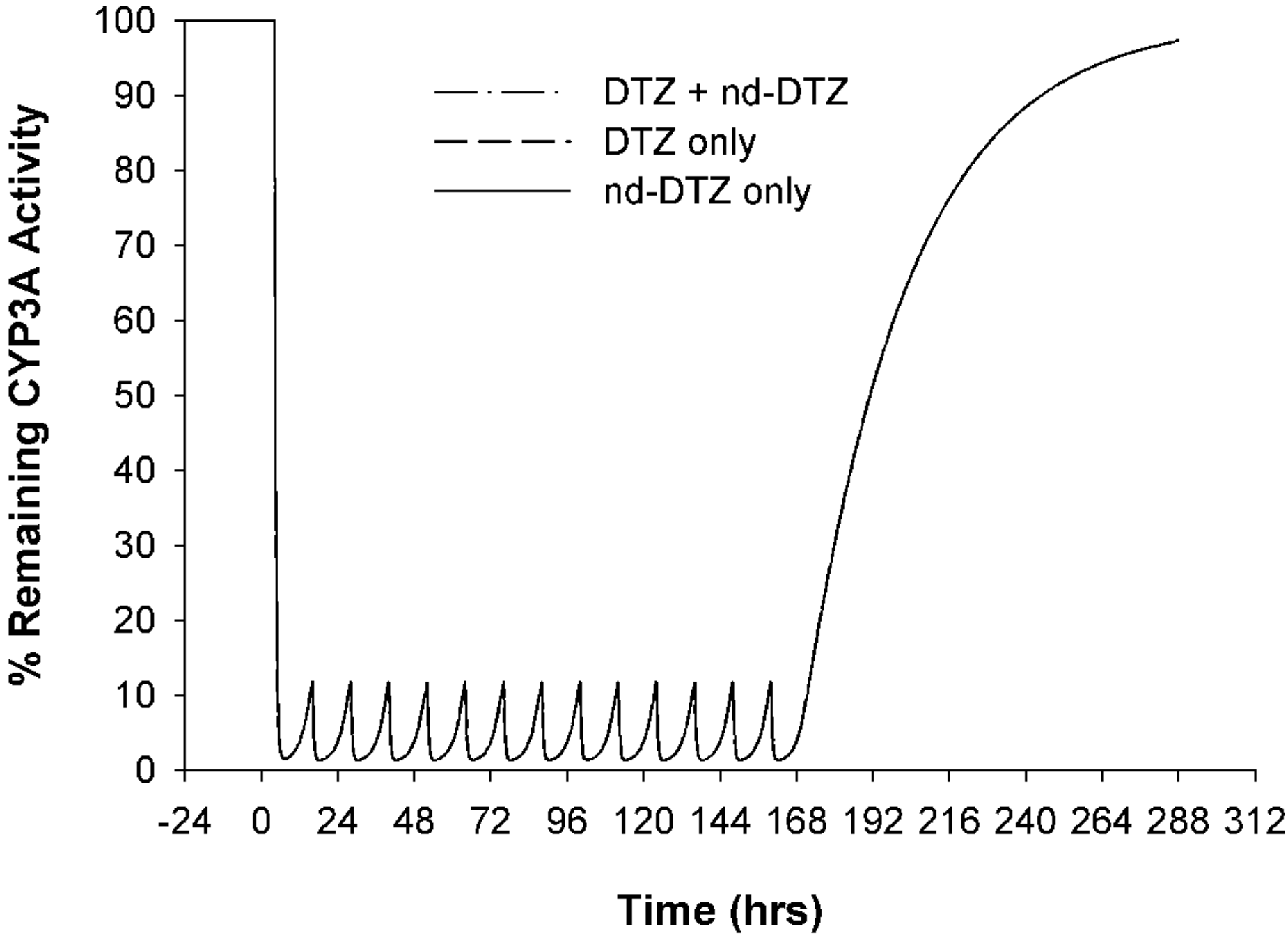
100
90
80
70
60
50
40
30
20
10
0
% Remaining CYP3A Activity
DTZ + nd-DTZ
DTZ only
nd-DTZ only
-24
0
24
48
72
96
120
144
168
192
216
240
264
288
312
Time (hrs)

DMD Fast Forward. Published on May 6, 2009 as DOI: 10.1124/dmd.109.026658
This article has not been copyedited and formatted. The final version may differ from this version.

Fig 6

C

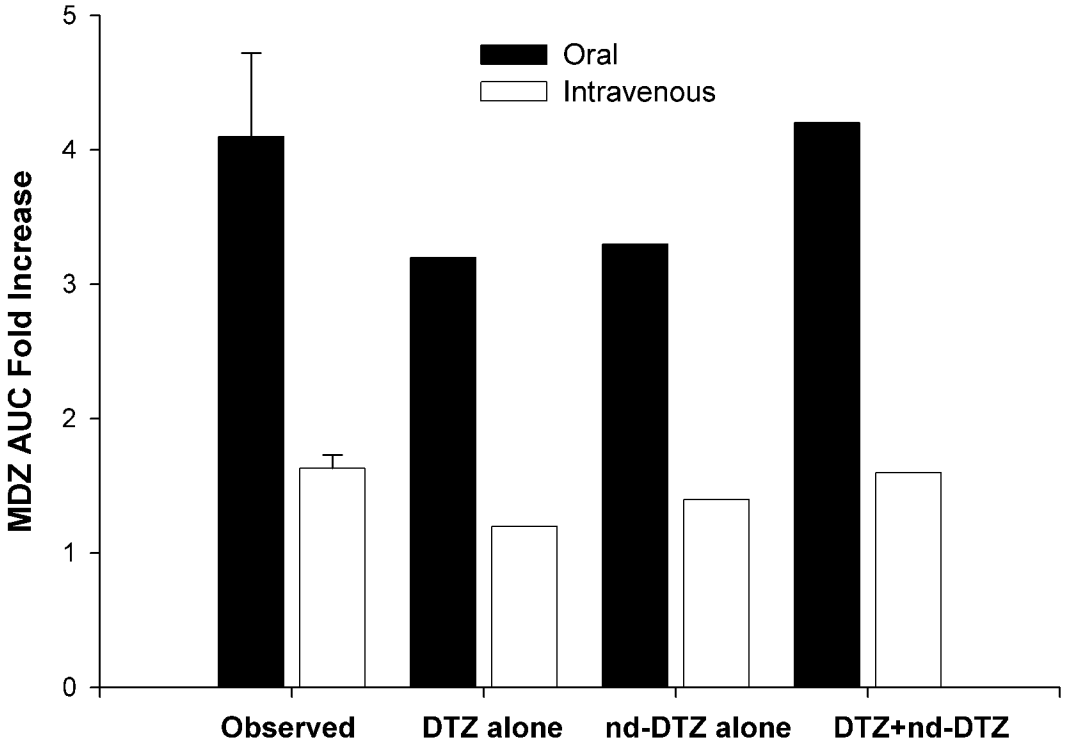

DMD Fast Forward. Published on May 6, 2009 as DOI: 10.1124/dmd.109.026658
This article has not been copyedited and formatted. The final version may differ from this version.

Fig 6

D

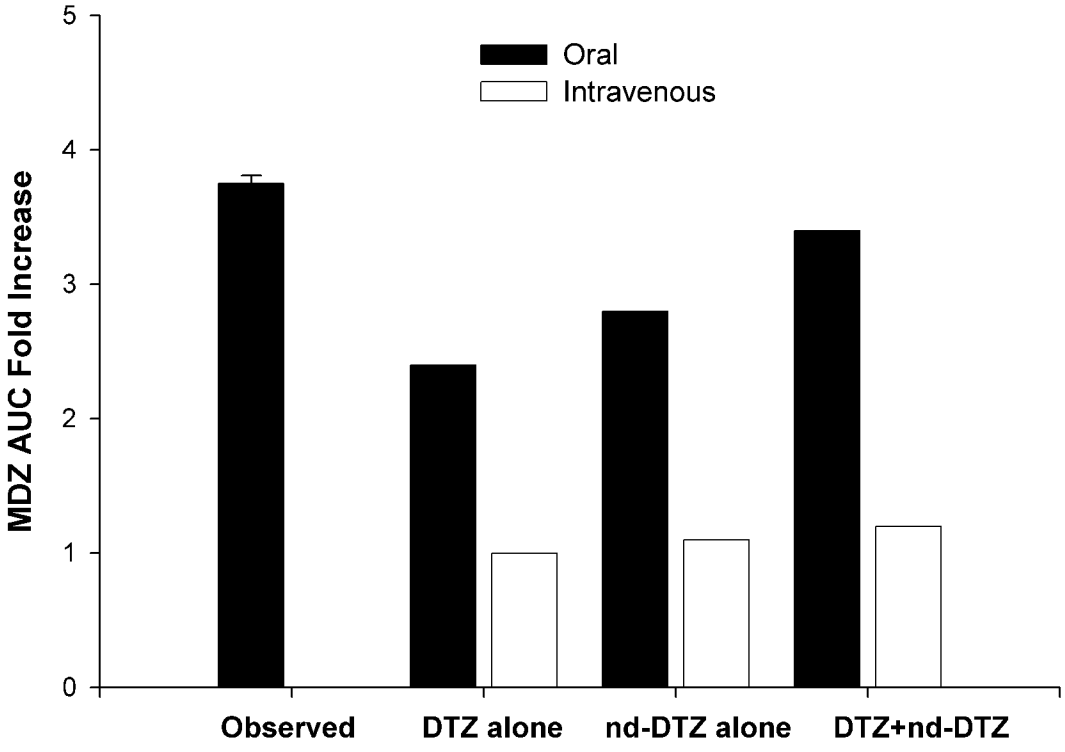

Figure 7

DMD Fast Forward. Published on May 6, 2009 as DOI: 10.1124/dmd.109.026658
This article has not been copyedited and formatted. The final version may differ from this version.